A Current Observer to Reduce the Sensor Count in Three-Phase PM Synchronous Machine Drives

Michael Eull, Mustafa Mohamadian, *Member, IEEE*, Daniel Luedtke, *Member, IEEE*, and Matthias Preindl, *Senior Member, IEEE*

***Abstract*—Reduced sensor systems are a topic receiving increasing attention as manufacturers seek to reduce costs by removing components from systems. One popular option is to remove phase current sensors and to estimate the missing currents using the ones remaining. This paper proves that it is possible to estimate the three-phase currents of an anisotropic permanent-magnet synchronous machine drive when only one-phase current sensor is present. The necessary conditions for observability and stability have been derived, providing certainty for the design of a permanent-magnet synchronous machine drive controller. The concept has been verified with high-fidelity simulations and experiments that show the one-phase current sensor observer is capable of controlling the drive system in the presence of sensor noise and significant parameter errors. The proposed phase current observer can be used to remove one sensor from a drive system by employing the two sensor observer with the one sensor observer acting as a failsafe.**

***Index Terms*—Estimation, linear systems, motor drives, observers, permanent-magnet (PM) machines.**

I. Introduction

The electrification of systems that were conventionally non-electric continues at a rapid pace, with the automotive industry being no different. One of the major factors holding back wider adoption of electrified vehicles is the cost, with a key metric for converters being the cost per kilowatt ($/kW) [1]. Thus, reducing the system cost is an important endeavor. Furthermore, safety has returned to the forefront with the advent of ISO 26262: Road Vehicles–Functional Safety [2]. To that end, a robust control strategy is critical, even if it means a cost reduction cannot be realized.

One means of reducing costs has been to remove sensors from the system by implementing sensorless or reduced sensor control strategies. The majority of studies have focused on removing the position sensor [3]–[5] and current sensors [6]–[13]. With respect to current sensor reduction, a plurality focus on removing all phase current sensors and replacing them with a single dc-link current sensor, placed between the capacitor and the semiconductors [6]–[9]. While this has the advantage of reducing the total sensor count by two, it also introduces inductance in the dc-link, leading to higher voltage stresses on the capacitors and transistors, as well as requiring a high bandwidth transducer. In this case, system simplification and cost reduction may not actually be realized.

An alternative to high bandwidth dc current sensors for zero-phase current sensor control is to consider the use of a wound rotor synchronous machine (WRSM) as opposed to a permanent-magnet synchronous machine (PMSM). As shown in [10], the use of the non-linear system enables the estimation of the three-phase currents through the knowledge of the position, speed, and the dc rotor excitation current of the WRSM alone.

To best overcome these issues, the current sensors should remain on the phase outputs, which is also the most widely employed approach to machine control. Most studies focus on reduced sensor counts for induction machines; however, several consider permanent magnet (PM) ones [11]–[13]. PMSMs are popular with OEMs thanks to their efficiency, mass, and power density advantages over other machine types [2]. In these three papers, all employ an observer in the case of one (or both) of the two current sensors encountering a fault, with the third (redundant) phase current sensor having been removed from the system.

The aforementioned studies have employed the concept of single current sensor control but have not been rigorous in their treatment of it. Indeed, in all three, observability is assumed to always be true, which may not necessarily be the case under any operating condition or even to begin with. Furthermore, the gain matrices applied in these works are provided as is with little derivation.

This paper builds upon previous works [11]–[14] by deriving the conditions for observability and stability, as well as providing thorough experimental validation of the algorithm in transient and steady-state conditions. Furthermore, the observer is shown to be capable of making a stable transition from two-to-one sensor operation, should a sensor failure occur during operation. Combined with the ability to reject sensor noise and parameter errors, the proposed linear phase current observer's robustness has been demonstrated.

Manuscript received December 17, 2018; revised March 14, 2019; accepted April 30, 2019. Date of publication June 2, 2019; date of current version August 14, 2019. Paper 2018-IDC-1323.R1, presented at the 2018 IEEE Transportation Electrification Conference and Expo, Long Beach, CA, USA, Jun. 13–15, and approved for publication in the IEEE Transactions on Industry Applications by the Industrial Drives Committee of the IEEE Industry Applications Society. *(Corresponding author: Michael Eull.)*

M. Eull and M. Preindl are with the Department of Electrical Engineering, Columbia University in the City of New York, New York, NY 10027 USA (e-mail: michael.eull@columbia.edu; matthias.preindl@gmail.com).

M. Mohamadian and D. Luedtke are with the "Electric Motor Integration & Controls" team, FCA US LLC, Auburn Hills, MI 48326 USA (e-mail: Mustafa.Mohamadian@fcagroup.com; daniel.luedtke@fcagroup.com).

Color versions of one or more of the figures in this paper are available online at http://ieeexplore.ieee.org.

Digital Object Identifier 10.1109/TIA.2019.2920804

II. Machine Model

The general state-space equations are written as

$$\dot{x}(t) = \mathbf{A}x(t) + \mathbf{B}u(t) \tag{1a}$$

$$y(t) = \mathbf{C}x(t) + \mathbf{D}u(t) \tag{1b}$$

where $\mathbf{A}$, $\mathbf{B}$, $\mathbf{C}$, and $\mathbf{D}$ are matrices related to the system at hand; $x(t)$ is the state vector and $\dot{x}(t)$ is its derivative; $u(t)$ is the input to the system; and $y(t)$ is the (measured) output of the system. Working in state space is conducive to both modeling and control.

A. Coordinate System Transformations

The Clarke transform moves the three-phase system to a two-phase stationary coordinate system, where the axes are orthogonal to one another. This transformation is performed as $x_{\alpha\beta} = \mathbf{T}x_{abc}$, where

$$\mathbf{T} = \frac{2}{3}\begin{bmatrix} 1 & -\frac{1}{2} & -\frac{1}{2} \\ 0 & \frac{\sqrt{3}}{2} & -\frac{\sqrt{3}}{2} \end{bmatrix}. \tag{2}$$

An additional transformation, the Park transform, can be performed to turn the stationary reference frame into a rotating one. The benefit of such an operation is that the electrical system is synchronized with this frame, making computations easier as the time-varying variables look like constants. It is performed as $x_{dq} = \mathbf{P}(\theta_e)x_{\alpha\beta}$, where

$$\mathbf{P}(\theta_e) = \begin{bmatrix} \cos\theta_e & \sin\theta_e \\ -\sin\theta_e & \cos\theta_e \end{bmatrix}. \tag{3}$$

When enacting the control, it becomes necessary to perform inverse transformations to go from the dq frame back to the abc frame for the generation of pulsewidth modulation duty cycles. The inverse Park transform is the transpose of the Park transform, i.e., $\mathbf{P}^{-1}(\theta_e) = \mathbf{P}^{\mathrm{T}}(\theta_e)$. The inverse Clarke transform requires more care as the matrix is not square. To handle this, one must use the Moore–Penrose pseudoinverse of $\mathbf{T}$, designated by the superscript $+$, which is defined as

$$\mathbf{T}^{+} = \frac{3}{2}\begin{bmatrix} 1 & 0 \\ -\frac{1}{3} & \frac{\sqrt{3}}{3} \\ -\frac{1}{3} & -\frac{\sqrt{3}}{3} \end{bmatrix}. \tag{4}$$

B. dq Dynamical Model

The linear dynamical model of the PMWM in the dq frame, can be written as [15]

$$L_d\dot{i}_d = v_d - Ri_d + \omega_e L_q i_q \tag{5a}$$

$$L_q\dot{i}_q = v_q - Ri_q - \omega_e L_d i_d - \omega_e\psi_r \tag{5b}$$

where v_d, i_d, and L_d and v_q, i_q, and L_q are the *d*- and *q*-axis voltages, currents, and inductances, respectively; R is the per-phase resistance of the stator windings; ψ_r is the flux of the PMs; ω_e is the electrical angular velocity, which is linked by the number of pole pairs, p, to the mechanical angular velocity, ω_r, by $\omega_e = p\cdot\omega_r$.

In (5), the system has been linearized by assuming that the mechanical time constants are much slower than the electrical ones and that the steady state has developed, i.e., $\dot{\omega}_r = 0$. These assumptions combine to simplify the model from a non-linear time-varying system to a linear time-invariant one, enabling an easier analysis and design of the control. In turn, this makes the machine's back electromotive force an exogenous input to the system, denoted by E. From this, we can convert (5) to state space and write the relevant matrices as

$$\mathbf{A} = -\mathbf{L}_{dq}^{-1}\left(R\mathbf{I} + \omega_e\mathbf{J}\mathbf{L}_{dq}\right)$$

$$\mathbf{B} = \mathbf{L}_{dq}^{-1}, \quad E = \omega_e\mathbf{L}_{dq}^{-1}\psi$$

where $\mathbf{L}_{dq} = \mathrm{diag}([L_d, L_q])$; $\mathbf{J} = [[0,1]^{\mathrm{T}}, [-1,0]^{\mathrm{T}}]$, which accounts for cross-coupling effects between the two axes; and $\psi = [0, \psi_r]^{\mathrm{T}}$.

III. Observability Analysis

Observability is the property that the states of the system can be reconstructed from the measured output. A system is observable if the observability matrix defined as

$$\mathbf{O} = \begin{bmatrix} \mathbf{C} \\ \mathbf{CA} \\ \vdots \\ \mathbf{CA}^{n-1} \end{bmatrix} \tag{6}$$

is of full *column* rank.

Observability of PMSM drives has previously been assessed in literature, though not in the same manner as what is presented in this paper. Indeed, the most comprehensive studies to date focused on the non-linear system for both current [10] and position [16] estimation, where it was rigorously shown that the machine's currents, position, and speed could be estimated under certain conditions. An equivalent assessment of observability for the linear time-invariant model of a PMSM is necessary to verify the feasibility of reduced sensor control.

Critical to the analysis is the $\mathbf{C}$ matrix and its definition. Typically, it defines what state(s) becomes the system's output(s). In this paper, it is modified to be comprised of two components: a so-called *sensor selection* matrix, $\mathbf{Q}$, which is used to designate what sensors are present in-system; and inverse coordinate system transformations, to move from $\alpha\beta$ or dq to abc. The system's output can then be written as

$$y(t) = i_{abc} = \mathbf{C}i = \mathbf{Q}\mathbf{T}^{+}\mathbf{P}^{-1}(\theta_e)\, i_{dq}. \tag{7}$$

The sensor selection matrix, $\mathbf{Q}$, has several permutations stemming from the basic form

$$\mathbf{Q} = \begin{bmatrix} phA & 0 & 0 \\ 0 & phB & 0 \\ 0 & 0 & phC \end{bmatrix} \tag{8}$$

where phA, phB, and $phC \in \{0, 1\}$ and denote the absence (0) or presence (1) of a sensor.

A. Three and Two Sensor Cases

Proposition 1: The system is always observable when either three or two sensors are present.

Proof: The $\mathbf{Q}$, $\mathbf{T}^{+}$, and $\mathbf{P}^{\mathrm{T}}(\theta_e)$ matrices all have rank 2. Thus, the observability matrix's rank is 2 and the system is observable. ■

B. One Sensor Case

Theorem 1: Let a motor drive have one current sensor on phase $k \in \{0, 1, 2\}$. The system is observable iff $L_\Delta \neq 0$ and

$$R\sin\left(2\theta_e - k\frac{4\pi}{3}\right) + 2\omega_e\left(L_\Sigma\cos\left(2\theta_e - k\frac{4\pi}{3}\right) - L_\Delta\right) \neq 0$$

with $L_\Delta = \frac{L_d - L_q}{2}$ and $L_\Sigma = \frac{L_d + L_q}{2}$.

Proof: Let $\mathbf{O}_k$ be the observability matrix. $\mathbf{O}_k$ is a square 2×2 matrix and has full rank iff $\det \mathbf{O}_k \neq 0$, where

$$\det \mathbf{O}_k = L_\Delta \times \left(\frac{R\sin\left(2\theta_e - k\frac{4\pi}{3}\right) + 2\omega_e\left(L_\Sigma\cos\left(2\theta_e - k\frac{4\pi}{3}\right) - L_\Delta\right)}{\left(L_\Delta^2 - L_\Sigma^2\right)}\right).$$

The denominator, $L_\Delta^2 - L_\Sigma^2$, can be removed since

$$L_\Delta^2 - L_\Sigma^2 = \left(\frac{L_d - L_q}{2}\right)^2 - \left(\frac{L_d + L_q}{2}\right)^2 = -L_d L_q \neq 0.$$

It is clear that the determinant is zero when either L_Δ or the inner term is zero. ■

An interesting result arises from this theorem: During operation, the system will become temporarily unobservable in some positions, which depends upon both the machine itself and its operating point. Corollary 1 goes into greater detail regarding this phenomenon for anisotropic PMSMs.

Corollary 1: With one current sensor present and $L_\Delta \neq 0$, the system is unobservable four times over a 2π period.

Proof: The electrical positions that render the system unobservable can be solved for by finding when the determinant is equal to zero by using the trigonometric identity $a\cos(x) + b\sin(x) = c\sin(x + \alpha)$, where $c = \sqrt{a^2 + b^2}$ and $\alpha = \arctan(\frac{a}{b})$. In this formulation, $a = 2\omega_e L_\Sigma$ and $b = R$. Thus, the unobservable angles are

$$\theta_{e,1} = \frac{1}{2}\left(\arcsin\left(\frac{2\omega_e L_\Delta}{c}\right) + k\frac{4\pi}{3} - \alpha\right) \tag{9a}$$

$$\theta_{e,2} = \theta_{e,1} + \pi \tag{9b}$$

$$\theta_{e,3} = \frac{1}{2}\left(\pi - \arcsin\left(\frac{2\omega_e L_\Delta}{c}\right) + k\frac{4\pi}{3} - \alpha\right) \tag{9c}$$

$$\theta_{e,4} = \theta_{e,3} + \pi. \tag{9d}$$

This corollary can also be proven graphically by plotting the determinant and its zero level set, as in Fig. 1. ■

The periodic position-dependent unobservability is not considered to be an issue in practice. When the machine is rotating, the system is observable on average and the observer will correct whatever errors may be injected by poor estimates during unobservable conditions; when the machine stops or stalls, the likelihood of stopping in one of the unobservable positions is infinitesimally small.

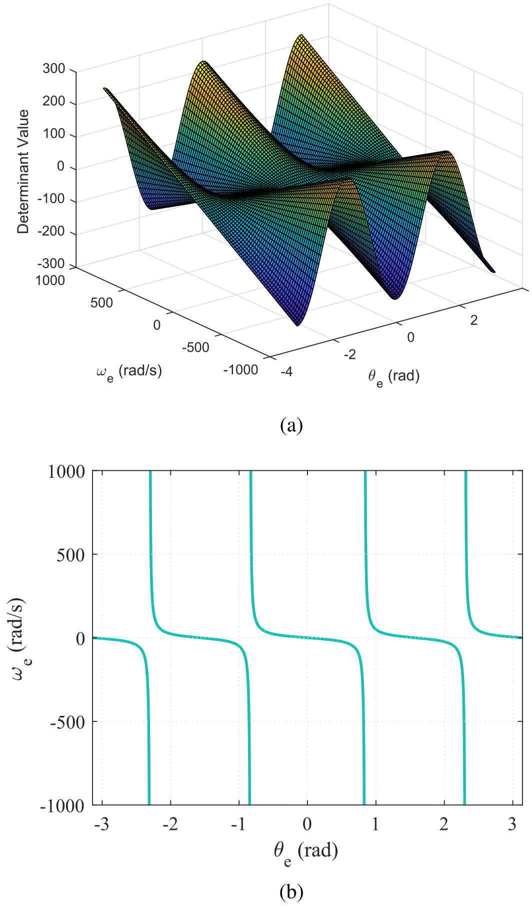

Fig. 1. Determinant of $\mathbf{O}_k$ and its zero level set. (a) Determinant evaluated over speed and position. (b) Zero level set.

C. Zero Sensor Case

This scenario is clearly unobservable. When no sensors are present, $\mathbf{Q}$ is zero, which forces $\mathbf{C}$ to zero. Consequently, the observability matrix is zero, which has rank zero.

IV. Observer

A. Model

The state-space model of (1) for an electric machine (i.e., $\mathbf{D} = 0$) can be rewritten with an observer as

$$\dot{\hat{x}}(t) = \hat{\mathbf{A}}\hat{x}(t) + \hat{\mathbf{B}}u(t) + \hat{E}(t) + \mathbf{L}e(t) \tag{10a}$$

$$\hat{y}(t) = \mathbf{C}\hat{x}(t) \tag{10b}$$

where the circumflex denotes an estimated quantity; $\hat{\mathbf{A}}$ is the model parameter matrix, which can deviate from the system matrix, $\mathbf{A}$; $e(t)$ is an error term that is the difference between the

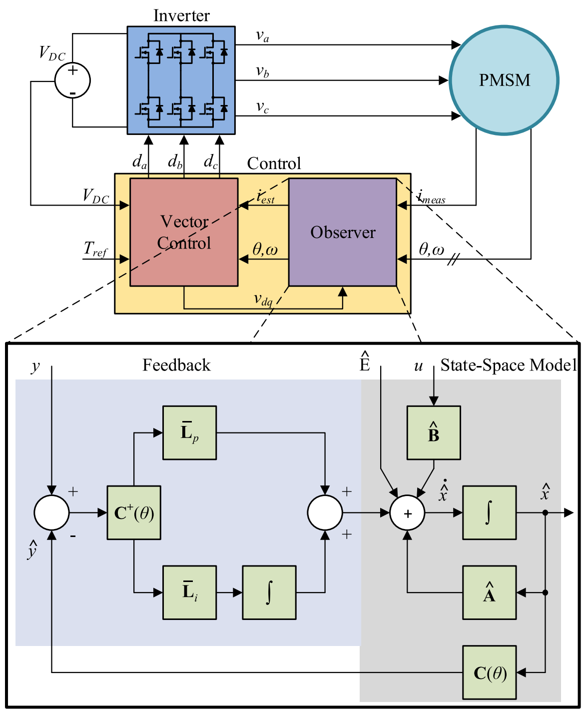

Fig. 2. System block diagram with the observer.

output of the system and the model, i.e., $e(t) = y(t) - \hat{y}(t) = \mathbf{C}(x(t) - \hat{x}(t))$; and $\mathbf{L}$ is a gain matrix, known as the *Luenberger gain*. Details of the structure of the observer itself are given in Fig. 2.

Defining the state error as $\tilde{x}(t) = x(t) - \hat{x}(t)$, it can be shown that

$$\dot{\tilde{x}}(t) = \dot{x}(t) - \dot{\hat{x}}(t) = (\mathbf{A} - \mathbf{LC})\,\tilde{x}(t). \quad (11)$$

Hence, for the system error to go to zero with no parameter mismatch ($\mathbf{A} = \hat{\mathbf{A}}$), all eigenvalues of $(\mathbf{A} - \mathbf{LC})$ must be less than zero. The Luenberger gain, $\mathbf{L}$, can be designed to place the system's poles to obtain a desired response. Proportional gain selection is discussed in detail in Section IV-C.

B. Robustness

Robustness concerns the observer's ability to sustain operation in the presence of modeling discrepancies. Generalizing the observer, the parameter matrix can be rewritten as $\mathbf{A} = \hat{\mathbf{A}} + \tilde{\mathbf{A}}$, where $\tilde{\mathbf{A}}$ is the error between the system and model. In this case, the error dynamics change from (11) to

$$\dot{\tilde{x}}(t) = \big(\hat{\mathbf{A}} - \mathbf{LC}\big)\tilde{x}(t) + \tilde{\mathbf{A}}x(t) + \tilde{\mathbf{B}}u(t) + \tilde{E}(t). \quad (12)$$

Thus, modeling error leads to an error in the system dynamics. In the dq frame, this is a constant error, which can be easily removed by the addition of an integral component. The impacts of this inclusion are discussed in Section IV-D.

C. Feedback Gain Selection

Proper selection of the Luenberger gain is critical to ensure system stability. Moreover, a certain response may be desired when a torque or speed change is commanded during operation. Both the stability and response of the PMSM are determined by $(\mathbf{A} - \mathbf{LC})$, as indicated by (11).

There is a caveat with respect to the definition of $\mathbf{L}$, which results from the definition of the error signal, $e(t) = y(t) - \hat{y}(t) = \mathbf{C}(x(t) - \hat{x}(t))$. In this formulation, the abc error is fed back into observer; however, the model being used is the dq one. Thus, $\mathbf{L}$ should contain a transformation to dq for proper compensation. This is achieved by defining $\mathbf{L} = \bar{\mathbf{L}}\mathbf{C}^{+}$; i.e., the product of a gain matrix and the pseudoinverse of $\mathbf{C}$. In the two sensor case, $\mathbf{C}^{+}\mathbf{C} = \mathbf{I}$, resulting in the error dynamics

$$\dot{\tilde{x}}(t) = (\mathbf{A} - \mathbf{LC})\,\tilde{x}(t) = \big(\mathbf{A} - \bar{\mathbf{L}}\big)\,\tilde{x}(t). \quad (13)$$

In the one sensor case, however, $\mathbf{C}^{+}\mathbf{C} \neq \mathbf{I}$. Expanding the compensation term gives $\mathbf{LC}$ to be

$$\frac{1}{2}\bar{\mathbf{L}}\left(\mathbf{I} + \begin{bmatrix} \cos\left(2\theta_e + k\frac{2\pi}{3}\right) & -\sin\left(2\theta_e + k\frac{2\pi}{3}\right) \\ -\sin\left(2\theta_e + k\frac{2\pi}{3}\right) & -\cos\left(2\theta_e + k\frac{2\pi}{3}\right) \end{bmatrix}\right). \quad (14)$$

The eigenvalues–and, particularly, those of the one sensor system–are difficult to assess and it becomes beneficial to consider their *boundaries*; that is, their maximum and minimum values. Weyl's inequality can be used for this purpose. Weyl's inequality places boundaries on the eigenvalues of a matrix by considering the sum of its Hermitian constituent components. Decomposing the system into Hermitian and non-Hermitian components can be rationalized by considering the eigenvalues of $\mathbf{A}$ alone: the off-diagonal elements primarily determine whether or not the eigenvalues are complex, whereas the diagonal elements primarily determine the real component. Because $\mathbf{A}$ is non-Hermitian, it is highly probable that the eigenvalues will be complex; thus, the real components become of primary interest, as they determine system stability, which are given by the Hermitian components.

Weyl's inequality specifies the upper and lower bounds on the eigenvalues of the sum of Hermitian matrices. Defining three Hermitian matrices, $\mathbf{X}$, $\mathbf{Y}$, and $\mathbf{Z}$, with eigenvalues χ, γ, and ζ, respectively, and describing the system as $\mathbf{Z} = \mathbf{X} + \mathbf{Y}$, Weyl's inequality states that

$$\zeta_{\max} \leq \chi_{\max} + \gamma_{\max}$$
$$\zeta_{\min} \geq \chi_{\min} + \gamma_{\min}.$$

It becomes necessary to decompose both $\mathbf{A}$ and $\mathbf{LC}$ into Hermitian and non-Hermitian components. Performing an exemplary operation on $\mathbf{A}$ gives

$$\mathbf{A} = \mathbf{A}_1 + \mathbf{A}_2 = \begin{bmatrix} -\frac{R}{L_d} & 0 \\ 0 & -\frac{R}{L_q} \end{bmatrix} + \begin{bmatrix} 0 & \omega_e\frac{L_q}{L_d} \\ -\omega_e\frac{L_d}{L_q} & 0 \end{bmatrix}. \quad (15)$$

This shows that the Hermitian component of $\mathbf{A}$ is $\mathbf{A}_1$. Similar operations can be applied to (14). For $\bar{\mathbf{L}}$ to be Hermitian, the simplest structure is a diagonal matrix. Noting that the two and one sensor cases have a different $\mathbf{LC}$, as per (13) and (14), means they must each have a different diagonal $\bar{\mathbf{L}}$. For the two sensor case, this results in $\bar{\mathbf{L}}_2 = \mathrm{diag}([L_1, L_2])$. In the one sensor case,

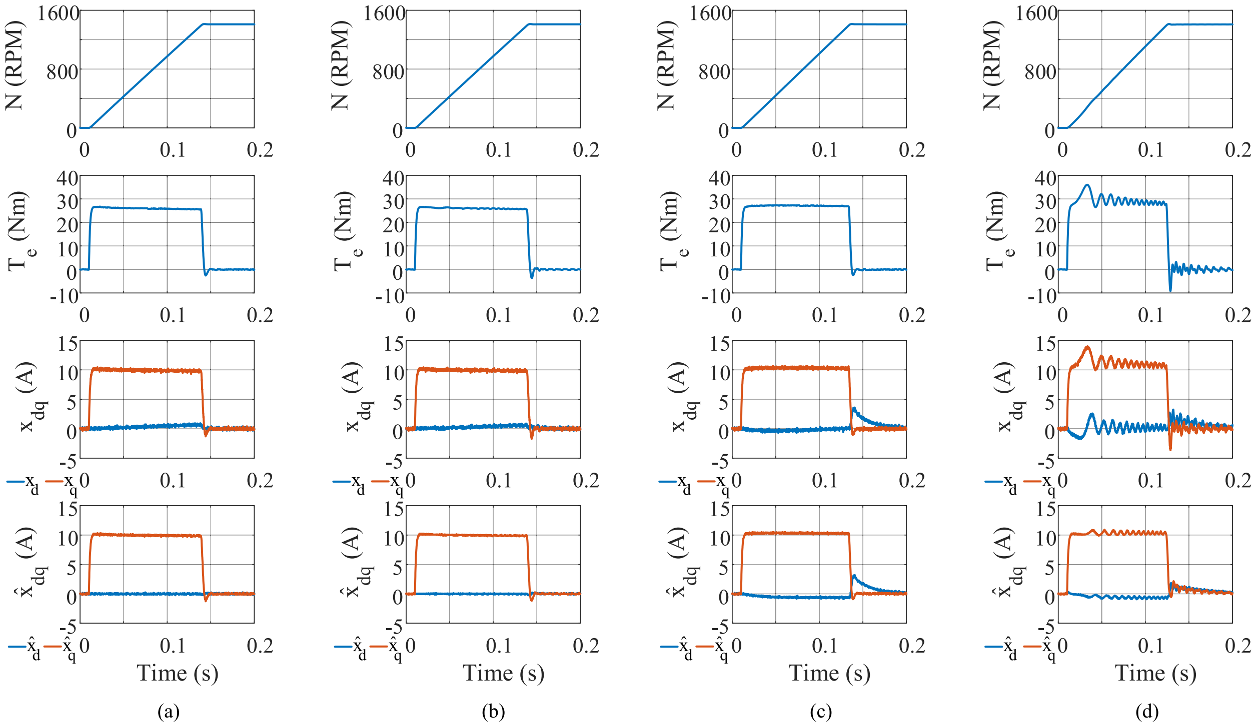

Fig. 3. Two and one sensor observer simulations during a speed step ($N = 0$ r/min $\rightarrow$ $N = 1400$ r/min at $t = 0.01$ s). Speed step performance sees little degradation, in spite of the oscillations the one sensor observer generates with parameter error. (a) Two sensor observer, no parameter error. (b) One sensor observer, no parameter error. (c) Two sensor observer, parameter error. (d) One sensor observer, parameter error.

by expanding (14), it can be seen that $\bar{\mathbf{L}}$ is Hermitian only if it is a diagonal matrix of one gain; that is to say, $\bar{\mathbf{L}}_1 = \mathrm{diag}([L_1, L_1])$.

$$\lambda_{\max,2} = \max\left\{-\frac{R}{L_d}, -\frac{R}{L_q}\right\} + \max\{-L_1, -L_2\} \tag{16a}$$

$$\lambda_{\min,2} = \min\left\{-\frac{R}{L_d}, -\frac{R}{L_q}\right\} + \min\{-L_1, -L_2\} \tag{16b}$$

$$\lambda_{\max,1} = \max\left\{-\frac{R}{L_d}, -\frac{R}{L_q}\right\} \tag{16c}$$

$$\lambda_{\min,1} = \min\left\{-\frac{R}{L_d}, -\frac{R}{L_q}\right\} - L_1. \tag{16d}$$

With this information in hand, Weyl's inequality can be applied and the boundaries of the eigenvalues determined for both the two and one sensor case. They are given by (16). Note that, in the one sensor case, only one extremity of the eigenvalues can be steered. This is a result of the rank deficiency of the system and results in the system's response time being dictated by the machine's $\frac{L}{R}$ time constant. In both the two and one sensor cases, the observer is guaranteed to be stable if and only if each $L_x \geq 0$.

D. Offset-Free Tracking

To remove steady-state offsets and errors, an integral component must be added to the control loop. This adds a second error dynamic to be assessed, which is the integral of the state error, $\tilde{x}_i$. The system dynamic model then becomes, omitting the input and exogenous input to the system for brevity

$$\begin{bmatrix} \dot{\tilde{x}} \\ \dot{\tilde{x}}_i \end{bmatrix} = \begin{bmatrix} \mathbf{A} - \bar{\mathbf{L}}_p\mathbf{C}^{+}\mathbf{C} & -\bar{\mathbf{L}}_i \\ \mathbf{C}^{+}\mathbf{C} & \mathbf{0} \end{bmatrix} \begin{bmatrix} \tilde{x} \\ \tilde{x}_i \end{bmatrix}. \tag{17}$$

To understand the system's response, the eigenvalues of this 4×4 matrix must be determined. One approach is to treat (17) as a block matrix and apply the Schur complement. The eigenvalues of a block matrix of the form

$$\mathbf{M} = \begin{bmatrix} \mathbf{M}_{11} & \mathbf{M}_{12} \\ \mathbf{M}_{21} & \mathbf{M}_{22} \end{bmatrix}$$

using the Schur complement, can be found by solving $\det(\lambda\mathbf{I} - \mathbf{M}_{11})\det(\lambda\mathbf{I} - \mathbf{M}_{22} + \mathbf{M}_{21}\mathbf{M}_{11}^{-1}\mathbf{M}_{12}) = 0$. This expression, however, is difficult to handle in practice, regardless of whether one or two sensors are present. Employing Weyl's inequality once more simplifies the problem greatly and yields the bounded

TABLE I
PMSM PARAMETERS

Parameter	Nominal Quantity	Introduced Error
Poles	10	-
Stator resistance (R)	0.4 Ω	-50%
d-axis inductance (L_d)	10.5 mH	+20%
q-axis inductance (L_q)	12.9 mH	+40%
Magnet flux (ψ_r)	0.3491 Wb	+10%

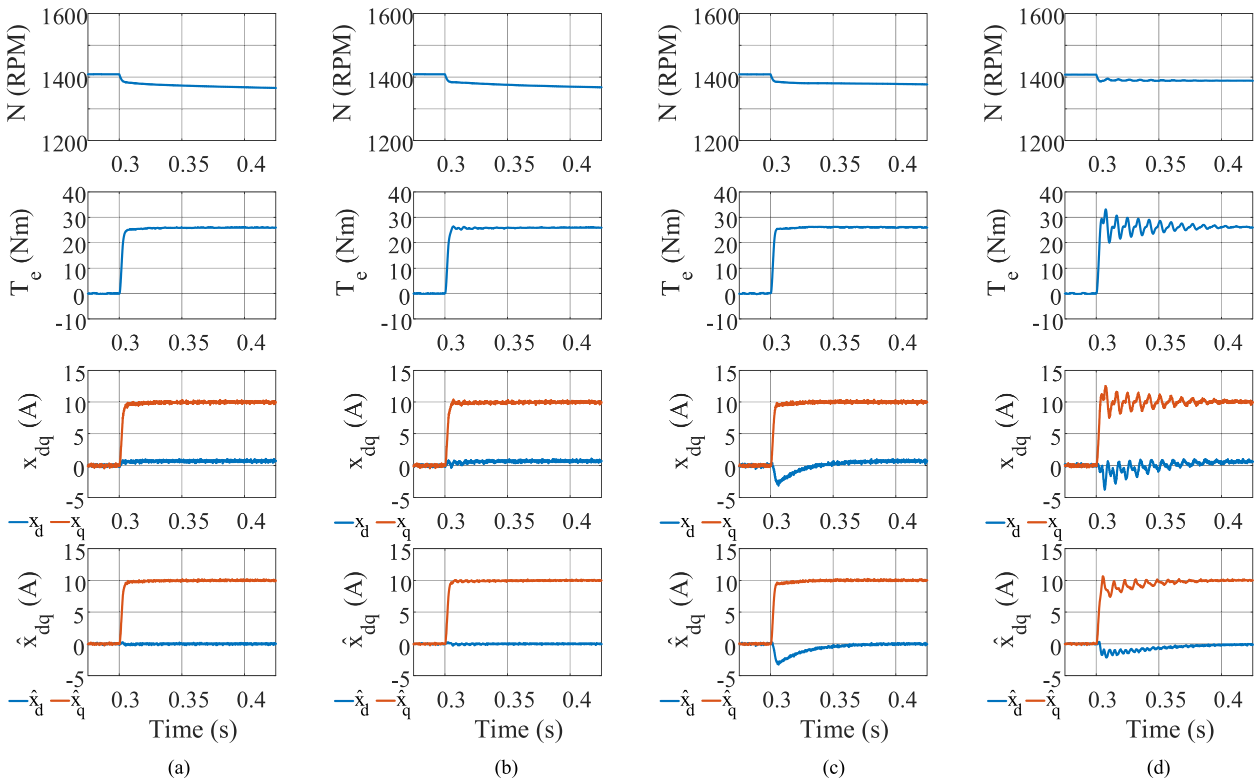

Fig. 4. Two and one sensor observer simulations during a torque step ($i_q = 0$ A $\rightarrow i_q = 10$ A at $t = 0.3$ s). The one sensor observer sees additional oscillations, which are amplified with parameter error, though steady-state operation is equivalent. (a) Two sensor observer, no parameter error. (b) One sensor observer, no parameter error. (c) Two sensor observer, parameter error. (d) One sensor observer, parameter error.

eigenvalues

$$\lambda_{\max,2} = 0 \tag{18a}$$

$$\lambda_{\min,2} = \min\left\{-\frac{R}{L_d}, -\frac{R}{L_q}\right\} + \min\left\{-L_1, -L_2\right\} \tag{18b}$$

$$\lambda_{\max,1} = 0 \tag{18c}$$

$$\lambda_{\min,1} = \min\left\{-\frac{R}{L_d}, -\frac{R}{L_q}\right\} - L_1. \tag{18d}$$

Several insights are gleaned regarding the observer's performance from these boundaries. First and foremost is that the maximum eigenvalue is zero, resulting from the addition of integrators. The presence of integrators then implies that the other two eigenvalues will be the same as the proportional case, given by (16). This line of reasoning can be verified by decomposing the 4×4 $\mathbf{A}$ matrix into its constituent Hermitian components and finding their respective eigenvalues. The key takeaway, however, is that the stability of the system is not impacted by the addition of an integral component.

V. Simulation Results

Simulations have been executed to validate the outlined observer design with machine parameters as in Table I on the system described by Fig. 2. Simulations with and without parameter error are enacted to assess baseline performance and the observer's ability to reject modeling discrepancies; for example, in applications where the machine parameters are not updated during operation via a look-up table or model.

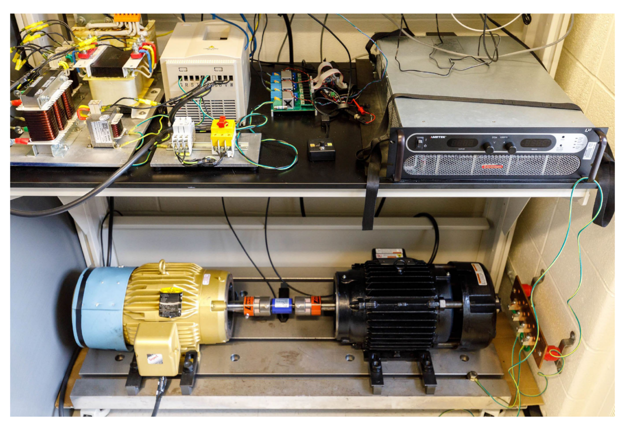

Fig. 5. Experimental setup.

The system is simulated with the one and two sensor observers providing the dq currents for the field-oriented control algorithm. Gaussian noise of approximately 0.6 A peak-to-peak (variance $\sigma^2 = 0.01$) is added to the current sensor(s) to assess whether the observers can operate well in the presence of noise. In the simulations, an initial speed command of 1400 r/min is made at $t = 0.01$ s, which is shown in Fig. 3. In Fig. 4, a 26 Nm torque command is made at $t = 0.30$ s. In both figures, it can be seen that the observers rapidly and accurately converge upon the desired current values. For the one sensor observer, transient oscillations

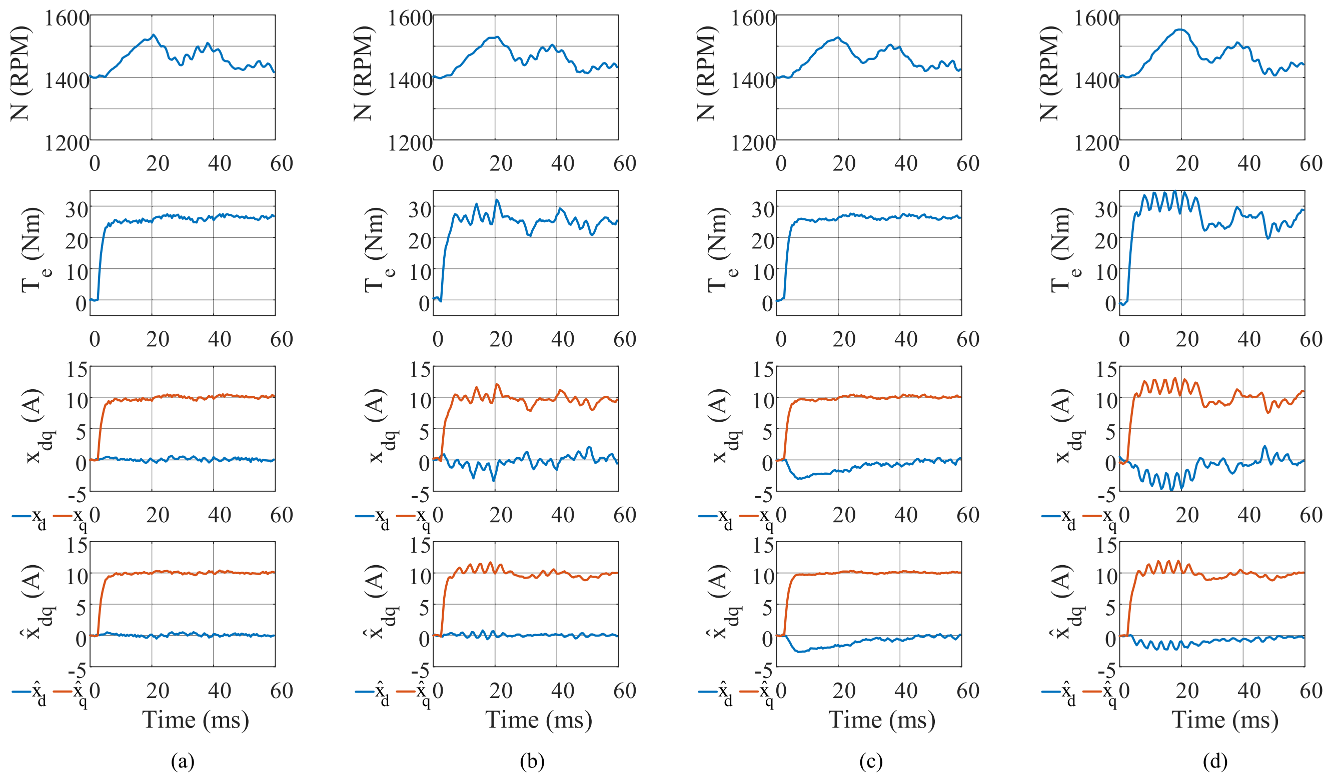

Fig. 6. Transient experimental validation ($i_q = 0\,\mathrm{A} \rightarrow 10\,\mathrm{A}$ at $t = 2.5$ ms): one and two sensor observers with and without parameter error. The one sensor observer has similar rise times, though the settling time, as a result of oscillations, is longer. (a) Two sensor observer, no parameter error. (b) One sensor observer, no parameter error. (c) Two sensor observer, parameter error. (d) One sensor observer, parameter error.

are most pronounced with large parameter error present, though they decay within 100 ms. The proposed observer is also capable of rapidly recovering from a controller reset transient, which is shown in [14].

VI. Experimental Results

The linear observer has been tested using the experimental setup in Fig. 5. The observer is evaluated on the PMSM with the parameters given in Table I and is interfaced with a custom-built silicon carbide MOSFET three-phase inverter [17]. The PMSM is connected to an induction machine driven by an industrial variable frequency drive in a dynamometer configuration.

A. General Operation

For control algorithm validation, both the two and one sensor observers were tested with both accurate and inaccurate parameters, as given in Table I. The dq current waveforms were captured and plotted during transient (step change) and steady-state operation, shown in Figs. 6 and 7, respectively.

The plots of Fig. 6 show a rapid convergence to the requested torque (i_q) value during transients; however, the one sensor observer encounters oscillations, which is a result of the incomplete $\mathbf{C}^+$ transformation. These oscillations are more pronounced with parameter error present, though they mostly decay over the 60 ms window captured. With parameter error, it can be seen that a temporary error in i_d arises, which is due to the parameter error also influencing the cross-coupling term used in the field-oriented control algorithm. The experimental results are consistent with the simulations presented in Fig. 4.

In the steady state (see Fig. 7), the difference between reference and measurement is small in all cases, even under one sensor operation with an omnipresent oscillatory term. Parameter error has minimal impact in this regime.

Two other performance metrics of value for the observer are its noise rejection capabilities and its ability to respond to changing conditions For the former, the observer was run in the steady state and the rms noise magnitude was computed from measurements; for the latter, the observer was reset ($\hat{x} = 0$) and the 10%–90% rise time was determined. The results are plotted in Fig. 8. For the two sensor observer, the tradeoff is clear: a higher gain ($\mathbf{L}_p$) translates to a faster response time but with more sensor noise coupling into the control. For the one sensor observer, things are less clear. In terms of noise, the sinusoidal term dominates at such low noise levels. With respect to rise time, it can be inferred that the feedback term $\mathbf{C}^+ e_{abc}$ creates a position-dependent response rate. If the position is favorable, the response will be swift; if the position is not, the response will be more gradual. Regardless of this nuance, an underlying trend towards a faster response with a higher $\mathbf{L}_p$ can still be seen.

A final point of interest for the current observer is the impact of parameter error on the system's steady-state performance. To assess this, the rms ripple current is calculated and used as a metric for performance, with the results given in Table II. In all cases, the one sensor observer performs worse than the two sensor observer and measurements alone, resulting from

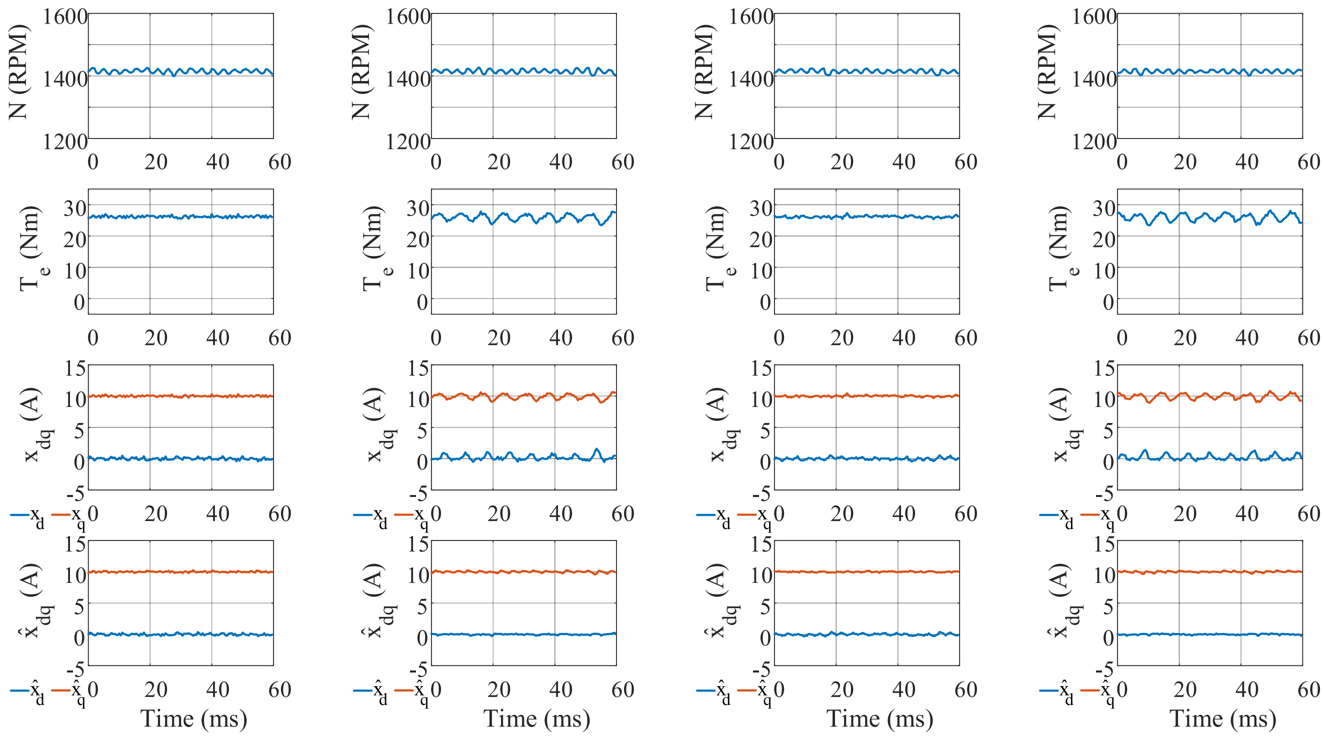

(a) (b) (c) (d)

Fig. 7. Steady-state experimental validation ($i_q = 10$ A): one and two sensor observers with and without parameter error. The one sensor observer sees a sinusoidal oscillation on the measurements as a result of the feedback term $\mathbf{C}^{+}(y - \hat{y})$. (a) Two sensor observer, no parameter error. (b) One sensor observer, no parameter error. (c) Two sensor observer, parameter error. (d) One sensor observer, parameter error.

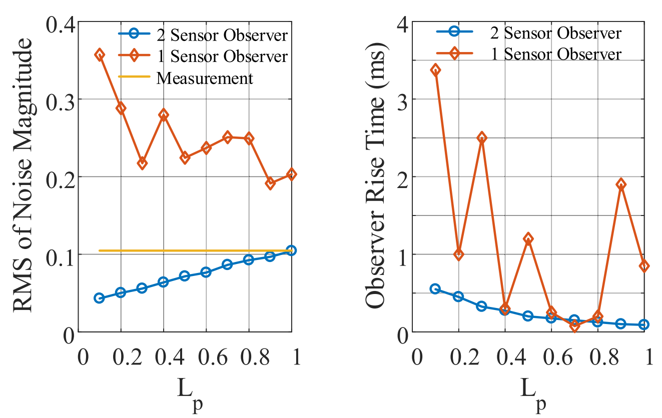

(a) (b)

Fig. 8. Observer performance as a function of observer gain $\mathbf{L}_p$: RMS noise and recovery time of the estimates ($\hat{x}$) after a forced reset ($\hat{x} = 0$). (a) RMS noise. (b) Estimate recovery time.

TABLE II
RMS RIPPLE CURRENT WITH VARYING PARAMETER ERROR

Parameter Case	Control Mechanism		
	Measurements	Two Sensor Observer	One Sensor Observer
Nominal	0.102	0.131	0.279
$0.8L_d$	0.115	0.126	0.275
$1.2L_d$	0.115	0.126	0.275
$0.6L_q$	0.115	0.126	0.275
$1.4L_q$	0.115	0.126	0.275
$0.9\psi_r$	0.115	0.126	0.275
$1.1\psi_r$	0.115	0.126	0.275
Table I Error	0.117	0.117	0.266

the sinusoidal error terms being fed back into the system. As a whole, the steady-state rms ripple current resulting from the use of the observers does not change significantly as parameters are changed.

The most notable performance degradation is in the over/undershoot and settling times of the dq currents when undergoing a step current (torque) change. This becomes most notable with the one sensor observer, where control over one eigenvalue is lost. When the observer overestimates the machine's parameters, the currents tend to overshoot; when the observer underestimates the parameters, the currents tend to undershoot.

B. Sensor Failure

The observer's ability to recover from a sensor fault and stably transition from two-to-one sensor operation is also demonstrated, with the result shown in Fig. 9. During this time, i.e., after the fault has occurred and before the switch to the one sensor observer has happened, one-phase current is as measured and the other is set to zero. This introduces an error into the control which, in turn, generates oscillations due to the sinusoidal feedback terms of the one sensor observer. The magnitude and duration of the oscillations are linked to the amount of time that the fault is present, as well as the gains applied to the system.

To demonstrate the impact of different Luenberger gains on oscillation magnitude and duration, simulations have been executed with varying values of $\mathbf{L}_p$ and are presented in Fig. 10.

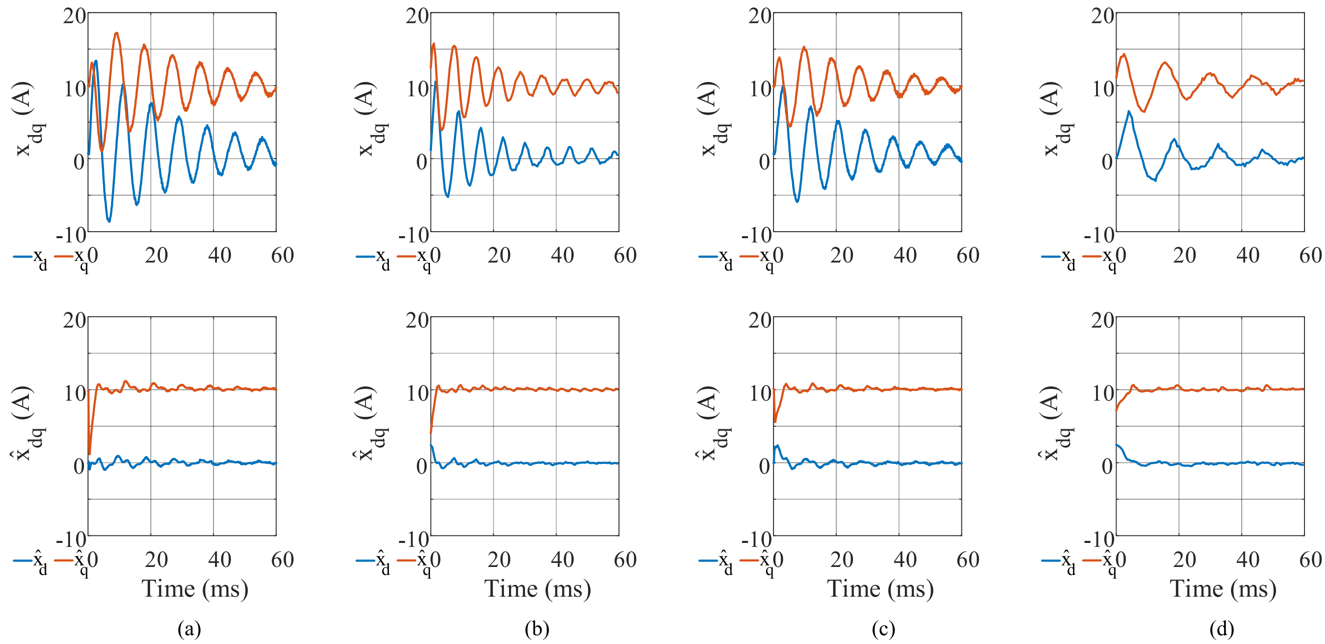

Fig. 9. Five switching cycle (500 μs) fault detection delay with and without parameter error. Parameter error does not necessarily increase oscillation amplitude; however, it does degrade the current waveforms. (a) Simulation, no parameter error. (b) Measurement, no parameter error. (c) Simulation, parameter error. (d) Measurement, parameter error.

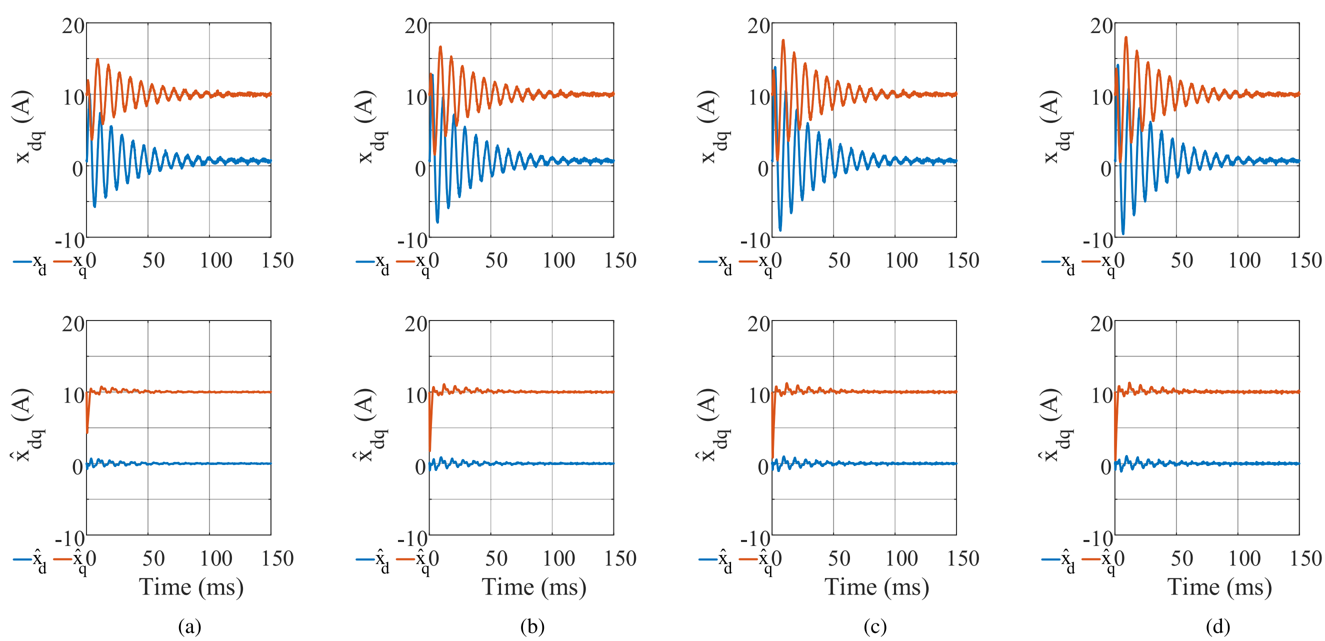

Fig. 10. Five switching cycle (500 μs) fault detection delay simulations with varying $\mathbf{L}_p$ values and without parameter error. Higher values of $\mathbf{L}_p$ increase the peak value of the oscillations. The settling time, however, remains roughly the same. (a) $\mathbf{L}_p = 0.2$. (b) $\mathbf{L}_p = 0.4$. (c) $\mathbf{L}_p = 0.6$. (d) $\mathbf{L}_p = 0.8$.

Higher values of $\mathbf{L}_p$ lead to larger oscillations than with a smaller $\mathbf{L}_p$; however, the disturbance duration remains roughly the same, irrespective of the gains assessed.

C. Algorithm Execution Time

The execution time of the linear observer is approximately 300 CPU cycles, equating to about 1.5 μs on the 32-b, 200 MHz DSP being used. It is expected that this number can be reduced through code optimization, increasing the observer's attractiveness to computationally constrained systems.

VII. Conclusion

This paper has proven that it is possible to reconstruct the three-phase currents of an anisotropic PMSM drive system using a single phase current sensor. These findings were substantiated with both simulations and experiments. This is a significant

Algorithm 1: Phase Current Observer.

1: **Measure** y_{abc}
2: **Transform** $\hat{y}_{abc} = \mathbf{C}\hat{i}_{dq}$
3: **Calculate** $e_{abc} = y_{abc} - \hat{y}_{abc}$
4: **Transform** $e_{dq} = \mathbf{C}^{+}e_{abc}$
5: **Compensate** $\dot{\hat{i}}_{dq} = \mathbf{A}\hat{i}_{dq} + \mathbf{B}v_{dq} + \hat{E}(t) + \mathbf{L}_p e_{dq} + \mathbf{L}_i \int e_{dq}$

departure from previous literature, which assumed it was possible to do so and showed it via experimentation. Both the conditions for observability and stability have been derived under two and one sensor operation, thereby providing a process by which a stable control system can be designed.

In terms of implementation, with three and two sensors in system, the observer can be used to filter the measurement noise, thereby enabling tighter control. If only one sensor is present, the three-phase currents can still be reconstructed at the expense of more noise in the control, a slower rise time and oscillations, the last of which are most prominent during system transients. Dependent upon the application, a savings of one or two sensors can be realized: the first, if the two sensor observer is employed with the one sensor observer acting as a failsafe mode; and the second, if the limitations of the one sensor observer are accepted and it is employed natively.

To facilitate implementation, pseudocode for the discussed current observer is given in Algorithm 1.

REFERENCES

[1] S. Rogers, "Electric drive status and challenges," 2012. [Online]. Available: http://www.energy.gov

[2] B. Bilgin *et al.*, "Making the case for electrified transportation," *IEEE Trans. Transp. Electrific.*, vol. 1, no. 1, pp. 4–17, Jun. 2015.

[3] Y. Sun, M. Preindl, S. Sirouspour, and A. Emadi, "Unified wide-speed sensorless scheme using nonlinear optimization for IPMSM drives," *IEEE Trans. Power Electron.*, vol. 32, no. 8, pp. 6308–6322, Aug. 2017.

[4] B. Nahid-Mobarakeh, F. Meibody-Tabar, and F.-M. Sargos, "Back EMF estimation-based sensorless control of PMSM: Robustness with respect to measurement errors and inverter irregularities," *IEEE Trans. Ind. Appl.*, vol. 43, no. 2, pp. 485–494, Mar./Apr. 2007.

[5] S. Nalakath, Y. Sun, M. Preindl, and A. Emadi, "Optimization-based position sensorless finite control set model predictive control for IPMSMs," *IEEE Trans. Power Electron.*, vol. 33, no. 10, pp. 8672–8682, Oct. 2018.

[6] M. Carpaneto, P. Fazio, M. Marchesoni, and G. Parodi, "Dynamic performance evaluation of sensorless permanent-magnet synchronous motor drives with reduced current sensors," *IEEE Trans. Ind. Electron.*, vol. 59, no. 12, pp. 4579–4589, Dec. 2012.

[7] J. I. Ha, "Current prediction in vector-controlled PWM inverters using single DC-link current sensor," *IEEE Trans. Ind. Electron.*, vol. 57, no. 2, pp. 716–726, Feb. 2010.

[8] H. Ye and A. Emadi, "A six-phase current reconstruction scheme for dual traction inverters in hybrid electric vehicles with a single dc-link current sensor," *IEEE Trans. Veh. Technol.*, vol. 63, no. 7, pp. 3085–3093, Sep. 2014.

[9] Y. Cho, T. LaBella, and J.-S. Lai, "A three-phase current reconstruction strategy with online current offset compensation using a single current sensor," *IEEE Trans. Ind. Electron.*, vol. 59, no. 7, pp. 2924–2933, Jul. 2012.

[10] A. Corne, N. Yang, J. Martin, B. Nahid-Mobarakeh, and S. Pierfederici, "Nonlinear estimation of stator currents in a wound rotor synchronous machine," *IEEE Trans. Ind. Appl.*, vol. 54, no. 4, pp. 3858–3867, Jul./Aug. 2018.

[11] Y.-s. Jeong, S.-K. Sul, S. E. Schulz, and N. R. Patel, "Fault detection and fault-tolerant control of interior permanent-magnet motor drive system for electric vehicle," *IEEE Trans. Ind. Appl.*, vol. 41, no. 1, pp. 46–51, Jan./Feb. 2005.

[12] G. H. B. Foo, X. Zhang, and D. M. Vilathgamuwa, "A sensor fault detection and isolation method in interior permanent-magnet synchronous motor drives based on an extended kalman filter," *IEEE Trans. Ind. Electron.*, vol. 60, no. 8, pp. 3485–3495, Aug. 2013.

[13] G. F. H. Beng, X. Zhang, and D. M. Vilathgamuwa, "Sensor fault-resilient control of interior permanent-magnet synchronous motor drives," *IEEE/ASME Trans. Mechatronics*, vol. 20, no. 2, pp. 855–864, Apr. 2015.

[14] M. Eull, M. Mohamadian, D. Luedtke, and M. Preindl, "A current observer to reduce the sensor count in three-phase PM synchronous machine drives," in *Proc. IEEE Transp. Electrific. Conf. Expo*, 2018, pp. 1–6.

[15] M. Preindl and S. Bolognani, "Optimal state reference computation with constrained MTPA criterion for PM motor drives," *IEEE Trans. Power Electron.*, vol. 30, no. 8, pp. 4524–4535, Aug. 2015.

[16] P. Vaclavek, P. Blaha, and I. Herman, "AC drive observability analysis," *IEEE Trans. Ind. Electron.*, vol. 60, no. 8, pp. 3047–3059, Aug. 2013.

[17] M. Eull, M. Preindl, and A. Emadi, "Analysis and design of a high efficiency, high power density three-phase silicon carbide inverter," in *Proc. IEEE Transp. Electrific. Conf. Expo*, 2016, pp. 1–6.

Authors' photographs and biographies not available at the time of publication.